# Thermal properties of a spin spiral: Manganese on tungsten(110)

G. Hasselberg,[1] R. Yanes,[1] D. Hinzke,[1] P. Sessi,[2] M. Bode,[2] L. Szunyogh,[3] and U. Nowak[1]
[1]*Fachbereich Physik, Universität Konstanz, D-78457 Konstanz, Germany*
[2]*Physikalisches Institut, Universität Würzburg, D-97074 Würzburg, Germany*
[3]*Department of Theoretical Physics and MTA-BME Condensed Matter Research Group, Budapest University of Technology and Economics, Budafoki út 8, H-1111 Budapest, Hungary*
(Received 24 July 2014; revised manuscript received 16 December 2014; published 2 February 2015)

We report a detailed study of the magnetic properties of a monoatomic layer of Mn on W(110). By comparing multiscale numerical calculations with measurements we evaluate the magnetic ground state of the system and its temperature-dependent evolution. We find that the ground state consists of a cycloidal spin spiral (CSS) that persists up to the Néel temperature with a temperature-independent wavelength. However, by continuously increasing the temperature, that CSS becomes thermally depinned. This results in a time-averaged absence of magnetic order, a process that can be viewed as the antiferromagnetic analog of superparamagnetism.

DOI: 10.1103/PhysRevB.91.064402 PACS number(s): 75.70.Ak

## I. INTRODUCTION

Low-dimensional magnetic systems have been widely reported to exhibit properties which cannot be obtained in bulk materials. The low coordination number and reduced symmetry as well as the possibility to induce strain by growing thin films on appropriate substrates results in a fascinating variety of complex magnetic ground states [1,2]. Of particular interest is understanding down to which size and up to which temperature these ground-state configurations can be considered stable. The dynamical magnetic behavior of nanomagnets is indeed of great interest for fundamental research as well as for its relevance in technological applications such as magnetic memories and sensors.

It is well known that thermally activated processes can trigger magnetization reversal and eventually completely destroy the magnetic order. These processes, which have been intensively investigated in nanosize ferromagnets [3], have remained largely unexplored in low-dimensional antiferromagnets and noncollinear spin structures. Experimentally, this is mainly due to the limited number of appropriate techniques. The development of spin-polarized (SP) scanning tunneling microscopy (STM) [4,5], however, made it possible to visualize the magnetic properties in real space with unprecedented resolution. This technique, initially used to study the magnetic ground state of bulk crystal surfaces [6,7] and thin films [8], was then rapidly applied to study a large variety of different magnetic systems like nanostructures [9–11] and domain walls [12,13], and in more recent years, it has been pushed to its ultimate limit: studies of the magnetic state of single atoms [14].

Variable-temperature STM measurements performed on a prototypical two-dimensional (2D) antiferromagnet, i.e., a monoatomic layer of manganese on tungsten(110) [called Mn/W(110) hereafter], reported on the observation of considerable size effects in the temperature-dependent onset of antiferromagnetic order [15]. The Mn/W(110) system is of particular interest since its ground state does not consist of a normal antiferromagnetic structure, with nearest-neighbor spins pointing along opposite directions, but is rather a cycloidal spin spiral propagating along the $[1\bar{1}0]$ direction with nearest-neighbor spins slightly canted ($\approx 7^\circ$). Its origin has been ascribed to the system's broken inversion symmetry, which in combination with relativistic effects induces a substantial Dzyaloshinskii-Moriya (DM) interaction. This interaction, discovered more than 50 years ago [16,17], has the form

$$E_{\mathrm{DM}} = -\sum_{i<j} \boldsymbol{D}_{ij} \cdot (\boldsymbol{s}_i \times \boldsymbol{s}_j), \tag{1}$$

where $\boldsymbol{s}_{i/j}$ denotes the normalized magnetic moments at sites $i/j$, and $\boldsymbol{D}_{ij}$ the corresponding DM vector. This interaction competes with the Heisenberg exchange and favors a noncollinear alignment of magnetic moments, being responsible for the formation of spin spirals [1,18], skyrmions [19,20], and particularly important for applications in some sample systems where the DM interactions may dominate exchange bias [21]. Recent studies have shown that thermal processes and the shape of the system [20,22] may modify the dynamics and mobility of the magnetic noncollinear state. This mobility has a fundamental importance for technological applications. Therefore a deeper understanding of the interplay between temperature and motion of textured magnets is needed.

Previous theoretical studies [1,18,23–25] investigated spin spirals in magnetic films utilizing *ab initio* calculations based on density functional theory. In the following, we will go beyond pure ground-state calculations and present an atomistic spin model with the parameters obtained from first-principles calculations to describe the magnetic properties of Mn/W(110). By means of spin-dynamics simulations, we first examine the cycloidal spin spiral (CSS) ground state and then focus on its temperature and size dependence. Additionally, the spin dynamics simulations allow us to analyze the thermally induced dynamical processes in the Mn/W(110) monolayer. Indeed, it is found that a successful comparison with temperature-dependent experiments can only be achieved if the dynamics of the CSS is taken into account.

 

## II. DETAILS OF REALIZATION

### A. Model and numerical approach

For the magnetic properties of the system Mn/W(110) we use a semiclassical, localized spin model,

$$\mathcal{H} = -\sum_{i<j} \boldsymbol{s}_i \mathcal{J}_{ij} \boldsymbol{s}_j - \sum_i \boldsymbol{s}_i \mathcal{K}_i \boldsymbol{s}_i - w \sum_{i<j} \frac{3(\boldsymbol{s}_i \cdot \hat{\boldsymbol{e}}_{ij})(\hat{\boldsymbol{e}}_{ij} \cdot \boldsymbol{s}_j) - \boldsymbol{s}_i \boldsymbol{s}_j}{r_{ij}^3}. \quad (2)$$

In the above Hamiltonian the first term represents the exchange energy in a general, relativistic form, the second term stands for the on-site anisotropy, and the last term is the magnetic dipole-dipole interaction. For the latter one it is $w = \mu_s^2 \mu_0 / 4\pi a^3$ with the vacuum permeability $\mu_0$, the atomic magnetic moment $\mu_s = 3.5\mu_B$ taken from our *ab initio* calculations, and the distance between sites $r_{ij}$ (normalized to the lattice constant along the [001] direction, $a = 0.3165$ nm, as taken from Ref. [8]) and the respective unit vector $\hat{\boldsymbol{e}}_{ij}$. Due to the $C2v$ point-group symmetry of the system, $\mathcal{K}_i$ introduces a biaxial on-site anisotropy. The exchange matrix $\mathcal{J}_{ij}$ can be decomposed as [18]

$$\mathcal{J}_{ij} = J_{ij}^{\mathrm{iso}} \mathcal{I} + \mathcal{J}_{ij}^{\mathrm{S}} + \mathcal{J}_{ij}^{\mathrm{A}}, \quad (3)$$

relating the isotropic part $J_{ij}^{\mathrm{iso}} = \frac{1}{3}\mathrm{Tr}\mathcal{J}_{ij}$ with the usual Heisenberg exchange and the symmetric, traceless part $\mathcal{J}_{ij}^{\mathrm{S}}$ with exchange anisotropy (also known as two-site anisotropy). $\mathcal{I}$ is the identity $3 \times 3$ matrix, and the antisymmetric part $\mathcal{J}_{ij}^{\mathrm{A}}$ of the exchange matrix leads to the DM interaction as expressed in Eq. (1).

To obtain the parameters for this model from first principles a scalar-relativistic self-consistent calculation was carried out for the paramagnetic state of a Mn monolayer on W(110) using the screened Korringa-Kohn-Rostoker (SKKR) method [26] and the disordered local moment (DLM) picture [27]. Here we took into account a layer relaxation of $-6.9\%$ of the Mn layer [8]. The potentials were treated within the atomic sphere approximation and valence orbitals were considered up to an angular momentum of $\ell = 3$. The on-site anisotropy parameters and the exchange interaction matrices were then obtained in terms of the spin-cluster expansion (SCE) technique as based on the relativistic disordered local moment (RDLM) theory [28]. This technique was applied successfully to study a variety of ultrathin magnetic films [29–31].

In Fig. 1 the isotropic exchange interactions $J_{ij}^{\mathrm{iso}}$, as well as the magnitude of the DM vectors $|\boldsymbol{D}_{ij}|$, are plotted as a function of the distance $r_{ij}$. Additionally, in Table I the calculated values of $J_{ij}^{\mathrm{iso}}$ and $|\boldsymbol{D}_{ij}|$ for the first five nearest neighbors are presented. The large negative nearest-neighbor (NN) isotropic exchange interaction ($-42$ meV) and the positive second and third NN isotropic interactions would lead to a checkerboard antiferromagnetic ordering. From the on-site and two-site anisotropy parameters provided by our SCE-RDLM calculations we calculated the magnetic anisotropy energies per unit cell, $E[1\bar{1}0] - E[110] = -1.86$ meV and $E[001] - E[110] = 0.34$ meV. Thus, in agreement with Refs. [1] and [18], this antiferromagnetic (AFM) state would prefer alignment with the $[1\bar{1}0]$ direction.

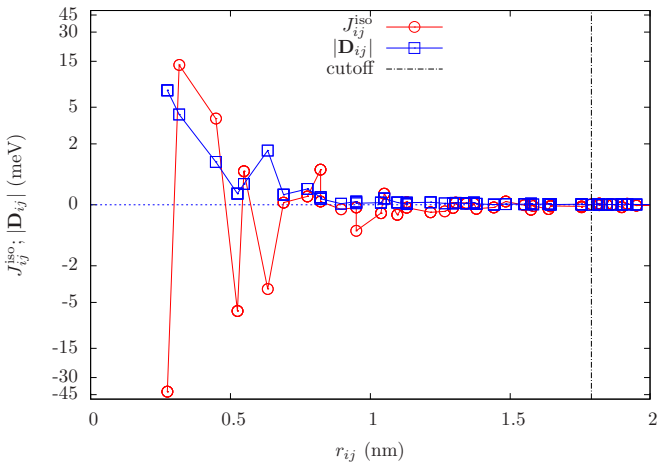


FIG. 1. (Color online) Calculated isotropic exchange interactions $J_{ij}^{\mathrm{iso}}$ and magnitudes of the DM vectors $|\boldsymbol{D}_{ij}|$ as functions of the distance between sites $i$ and $j$. Please notice the hyperbolic scaling of the $y$ axis. The vertical dashed line indicates the cutoff distance for our spin-dynamics simulations.

This magnetic structure is, however, modulated by the DM interactions as large as 7.5 meV in magnitude for the first NN. Note that the calculated parameters differ remarkably from those reported in Ref. [18] since (i) in the previous work the geometrical relaxation of the Mn layer was not taken into account and (ii) the relativistic torque method [32] based on a metastable ferromagnetic state was used instead of the SCE-RDLM method employed here. In this latter approach, due to the magnetically disordered host medium, the interactions decay rapidly with the distance, as clearly seen in Fig. 1. For this reason, in our subsequent simulations the different contributions to the tensorial exchange interaction, Eq. (3), were considered only for neighbors within a radius of $8a_x$, with $a_x = \sqrt{2} \cdot a/2$ the lattice constant along the $[1\bar{1}0]$ direction. The criteria to choose this cutoff of the exchange interaction was that it should be larger than $3a_x$, the value at which the periodicity of the CSS is stabilized.

Due to $C2v$ point-group symmetry, all the DM vectors lie in plane and exhibit, in general, both $x$ and $y$ components. The calculated DM vectors are displayed in Fig. 2 up to the fifth NN shell. Note again that this picture also differs from the corresponding entry in Fig. 1 of Ref. [18]. Eventually, the nonvanishing $x$ components of the DM vectors may lead to the occurrence of spin structures other than the CSS, e.g., helical spin spirals [23].

To study the ground-state properties along with those at elevated temperatures we solve the stochastic Landau-Lifshitz-

TABLE I. Calculated isotropic exchange interactions $J_{ij}^{\mathrm{iso}}$ and magnitudes of the DM vectors $|\boldsymbol{D}_{ij}|$ (all in meV) for the first five nearest neighbors (NNs).

| NN | 1 | 2 | 3 | 4 | 5 |
|---|---|---|---|---|---|
| $J_{ij}^{\mathrm{iso}}$ | $-41.98$ | 13.72 | 3.79 | $-6.14$ | 0.88 |
| $\lvert\boldsymbol{D}_{ij}\rvert$ | 7.51 | 4.2 | 1.2 | 0.26 | 0.49 |

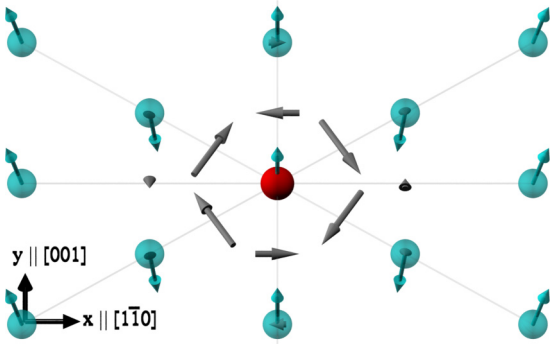


FIG. 2. (Color online) Sketch of the calculated DM vectors $\boldsymbol{D}_{ij}$ up to the fifth NN shell of the 2D lattice formed by the Mn atoms. The DM vectors (grey arrows) are placed at the center of the line connecting the center atom (red sphere) and its corresponding neighbor (green sphere). The length of the DM vector is proportional to its magnitude and also reflects the orientation in space. Note the rapid decay in the magnitude of DM vectors with distance; see also Fig. 1. Green arrows represent the magnetic moment.

Gilbert (SLLG) equation,

$$\frac{\partial \boldsymbol{s}_i}{\partial t} = -\frac{\gamma}{(1+\alpha^2)\mu_s}\boldsymbol{s}_i \times (\boldsymbol{H}_i + \alpha\, \boldsymbol{s}_i \times \boldsymbol{H}_i), \tag{4}$$

by means of Langevin dynamics, using a Heun algorithm [33,34]. The SLLG includes the gyromagnetic ratio $\gamma$, a phenomenological damping parameter $\alpha$ (high damping limit, $\alpha = 1$) and the effective field,

$$\boldsymbol{H}_i = \boldsymbol{\zeta}_i(t) - \frac{\partial \mathcal{H}}{\partial \boldsymbol{s}_i}, \tag{5}$$

which considers the influence of a temperature $T$ by adding a stochastic noise term $\boldsymbol{\zeta}_i(t)$, obeying the properties of white noise [35]:

$$\langle \boldsymbol{\zeta}_i(t) \rangle = 0; \tag{6}$$

$$\left\langle \zeta_i^{\eta}(t)\zeta_j^{\theta}(t') \right\rangle = \frac{2k_B T\alpha\mu_s}{\gamma}\delta_{ij}\delta_{\eta\theta}\delta(t-t'). \tag{7}$$

Here $i$, $j$ denote lattice sites and $\eta$ and $\theta$ Cartesian components of the stochastic noise.

In our simulations we consider open boundary conditions. Additionally, a fast Fourier transform (FFT) technique was implemented in the code, to efficiently trace tensorial exchange and dipole-dipole interactions and to perform a data analysis in reciprocal space. Another advantage of the use of the FFT technique is the considerable reduction of the computational time of our simulations. The FFT yields a landscape of intensities at different wave vectors corresponding to different real-space wavelengths λ. Intensity peaks thus reflect a distinct periodicity and allow for the measurement of the wavelength of the CSS in Mn/W(110) and also its decay with temperature. The magnitude of the peak square-root intensity ($I^{1/2}$), which naturally translates to the ground-state wavelength, is taken as the order parameter.

### B. Experimental setup and procedures

The experiments have been performed in an ultrahigh vacuum (UHV) system (base pressure $p < 1 \times 10^{-8}$ Pa) with two separate chambers for sample preparation and variable-temperature scanning tunneling microscopy. The W(110) crystal is prepared by numerous cycles of long-term heating at 1500 K in an oxygen atmosphere $p_{\mathrm{Ox}} = 10^{-6} \ldots 10^{-4}$ Pa and subsequent flashing up to 2400 K [36]. Mn was evaporated from a tungsten crucible heated by electron bombardment.

Our variable-temperature scanning tunneling microscope (VT-STM) allows for sample temperatures between 40 K and about 400 K. Irrespective of the particular sample temperature the tip always remains at room temperature. All data presented below were obtained in the constant-current mode of operation. Spectroscopic information is gained by measuring the derivative of the tunneling current $I$ with respect to the applied sample bias $U$. This so-called $dI/dU$ signal is, to a first-order approximation, proportional to the local density of states (LDOS) of the sample below the tip apex [37]. Experimentally, the $dI/dU$ signal is obtained by adding a small bias modulation (typically 10 mV) to the the bias voltage and detecting the resulting modulation of the tunneling current by lock-in technique.

In the experimental part of this contribution we probe the existence or absence of the cycloidal spin spiral in Mn/W(110) by making use of the so-called spin-orbit contrast (SOC). As has been described in Refs. [15,38] the strong spin-orbit coupling in Mn/W(110) leads to enhanced (reduced) electronic LDOS over in-plane (out-of-plane) magnetized regions. For Mn/W(110) the strongest SOC signal is usually observed at $U = +150$ mV. By sensing the modulation of the LDOS by means of the local $dI/dU$ signal measured with STS the spin spiral can even be detected with nonmagnetic tips. This SOC mode has two advantages which are particularly important for temperature-dependent studies where drift and occasional tip changes may affect the acquisition of high-resolution SP-STM data: (i) the existence of the spin spiral in Mn/W(110) can be detected even with nonmagnetic tips and (ii) it is no longer required to obtain atomic resolution since the cycloidal spin spiral exhibits a wavelength well above 10 nm.

## III. RESULTS AND DISCUSSION

### A. Ground state of Mn/W(110)

For finding the ground state of our Mn/W(110) model in terms of spin-dynamics simulations a cooling process was used. A monolayer of Mn atoms was modeled by a 2D centered rectangular lattice of 512 × 512 Mn spins. Starting with a random spin configuration at high temperature the system was thermalized at successively smaller temperatures until 0 K was reached. As a result the magnetic configuration consists of two AFM-coupled sublattices, each of which has their neighboring magnetic moments slightly tilted so that every row features a CSS along the $x$ direction ($\boldsymbol{k} \parallel [1\bar{1}0]$). The periodicity of the CSS is reflected in the $s_z$ (or in the $s_x$) component of the magnetic moments. The 2D space FFT of the $z$ component of the magnetization of Mn atoms leads to an intensity landscape with four peaks. These four peaks are equivalent, equally periodicity, intensity, and thermal dependence. For that reason

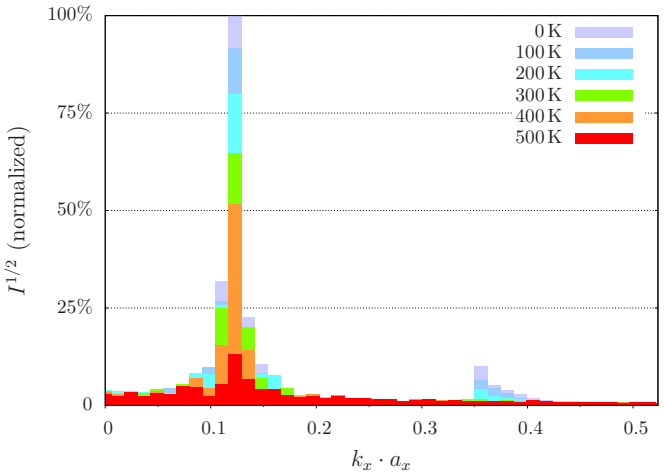


FIG. 3. (Color online) Spectrum of the $z$ component of the magnetic moments, defined as the normalized square root of the magnitude of the Fourier components, plotted over $k_x$, at $k_y = 2\pi/a$, for different temperatures. The high peak at around $k_x = 0.12/a_x$ indicates the periodicity of the spin spiral. The small peak around $k_x = 0.35/a_x$ is caused by the distortion of the sinusoidal ordering due to anisotropy contributions.

we choose only one, located at $(k_x = 0.12/a_x;\ k_y = 2\pi/a)$, to analyze the numerical periodicity and the thermal decay of the cycloidal spin spiral state. $k_y = 2\pi/a$ indicates the ferromagnetic order along the $y$ direction, and $k_x = 0.12/a_x$ shows a modulation along the $x$ direction corresponding to a value of $\lambda = 12 \pm 1$ nm; see Fig. 3. A direct fit of $s_z(x)$ to the theoretical function for a homogeneous CSS showed the same periodicity.

To check the role of the dipole-dipole interaction in the formation of the CSS in the Mn/W(110) system, we repeated the previous simulation neglecting the dipole-dipole interaction. Our simulations showed no effect of the magnetic dipole-dipole interaction on the periodicity of the CSS (in contrast to the case of Fe/W(110) [2]). The anisotropy contributions can, however, notably change the shape of the ground state, making the CSS not perfectly homogeneous, as the spins tend to align with the easy axis, parallel to the $[1\bar{1}0]$ direction. This leads to the second, smaller peak in Fig. 3. This peak corresponds with the third harmonic in the $x$ direction.

For comparison, we also employed the analytical approach of Bode *et al.*[1] to express the energy of an infinite, perfectly homogeneous, one-dimensional CSS as a function of $\lambda$,

$$E_{\mathrm{CSS}}(\lambda) = J\lambda^{-2} + D\lambda^{-1} + K/2. \tag{8}$$

We approximate $J$ and $D$ in the long-wavelength limit of our spin model as $J = \pi^2 \sum_j^{4\mathrm{thNN}} J_{ij}^{\mathrm{iso}} x_{ij}^2$ and $D = \pi \sum_j^{4\mathrm{thNN}} D_{ij}^{y} x_{ij}$, where $x_{ij}$ is the $x$ component of the position vector connecting sites $i$ and $j$. Note that the $y$ component of the DM vector is critical for a spin-spiral formation along $[1\bar{1}0]$ [23]. Equation (8) is minimized by $\lambda = -2J/D$, which yields $\lambda \approx 11.3$ nm for our parameters. In Ref. [1] simulation results were presented using parameters obtained by fitting the *ab initio* energy of spin spirals to Eq. (8) and a theoretical wavelength of $\lambda \approx 8$ nm was found. In terms of Monte Carlo simulations with spin-model parameters calculated via the relativistic torque method as based on the ferromagnetic state of the system, Udvardi *et al.* [18] obtained $\lambda \approx 7.2$ nm. We conclude that, as compared with previous theoretical attempts, our model clearly improved the agreement with the experimentally observed magnetic ground state of Mn/W(110) [1,15].

### B. Thermal properties

#### 1. Theory

For the investigation of the magnetic order of Mn/W(110) at finite temperature the system was first initialized in its ground-state magnetic configuration as obtained beforehand and then thermalized step by step towards elevated temperatures. For each temperature after a thermalization time the intensity landscape obtained from the FFT is calculated after each time step $\Delta t = 1 \times 10^{-15}$ s, and the time average is evaluated. This annealing procedure was done three times, each time starting with a different random seed for the stochastic term (thermal noise). The box plot in Fig. 3 depicts the square root of intensities in reciprocal space averaged in time and over the multiple trajectories.

The distinct peak centered around $(k_x = 0.12/a_x;\ k_y = 2\pi/a)$ is always visible in the intensity spectrum with comparably small noise even at elevated temperatures. This peak indicates the periodicity of the CSS. Obviously, the magnetic order decays and the spectrum widens in $k_x$ and $k_y$ with increasing temperature, while the wavelength of the CSS remains constant as can be recognized by the unchanged peak position. The fact that only a narrow range of $k_x$ and $k_y$ shows a significant temperature dependence may indicate that the two most relevant free-energy contributions, coming from isotropic exchange and DM interactions, should have the same thermodynamic temperature dependence.

#### 2. Experiment

This theoretical finding of a periodicity of the magnetic structure which is temperature independent over a broad range of temperatures is in good agreement with the experimental results presented in Fig. 4. The images report differential conductivity maps obtained on Mn/W(110) at different temperatures. A periodic modulation of the local density of states (LDOS), which unambiguously indicates the presence of the cycloidal spin spiral of Mn/W(110), is clearly visible at low temperatures.

Within error bars, the magnetic periodicity remains constant up to $T = 190$ K [see Fig. 4(a)]. No further evolution of the FFT intensity is detected for temperatures below $T = 40$ K. Indeed, data obtained using a low-temperature STM operated in a He-bath cryostat at a base temperature of $T = 10$ K show no significant change with respect to the data obtained at $T = 40$ K, which is the lowest temperature achievable in our variable-temperature STM. At temperatures above $T = 200$ K no periodic modulation can be detected in real space. This observation is corroborated by a reciprocal space analysis of the data, which was performed by FFT of line sections taken along the $[1\bar{1}0]$ direction, i.e., perpendicular to the stripes (not shown here). As depicted in Fig. 4(b), the intensity of the

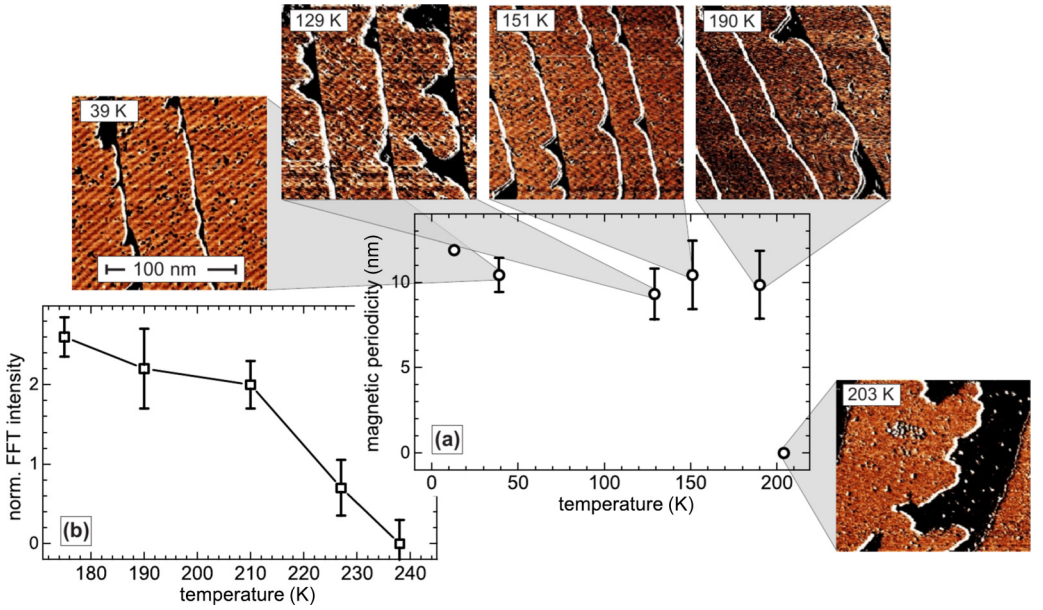


FIG. 4. (Color online) Measured periodicity of the CSS in Mn/W(110) as a function of temperature. The temperature-dependent behavior of the differential conductivity maps reported in the insets has been analyzed both in (a) real space and (b) by analyzing the intensity of the FFT peak associated with the CSS.

peak, which signals the presence of cycloidal spin spiral order, dramatically drops above $T = 210$ K, and completely vanishes at $T = 240$ K.

From the disappearance of the peak in the intensity spectra, we conclude that the experimentally determined Néel temperature $T_N$ is approximately 240 K, a value which is significantly below the onset of magnetic order at about 510 K as observed by our model calculations. As we will show later on, this apparent disagreement is related to the strongly different time scales which are probed in STM measurements as compared to model calculations, i.e., seconds versus nanoseconds. Indeed, it is well known that the question if magnetic order can be observed strongly depends on the time scale at which a system is probed. This point will be discussed in detail in the following section.

### C. Comparison between numerical and experimental Néel temperatures

Our dynamical simulations show that the CSS which is practically a static configuration at low temperature starts moving when the temperature is increased. A similar effect can be found for skyrmions in the presence of pinning traps at finite temperature, where the thermal fluctuation favors the skyrmions motion, increasing their mobility [39,40]. Occasionally, the initial CCS switches even to another CSS state with the same wavelength λ but with the magnetization of the two magnetic sublattices swapped. The frequency of this switching increases with temperature in such a way that at high temperature the system behaves similar to a superparamagnetic nanoparticle.

The thermally excited process of the CSS may explain the apparent discrepancy between numerical and experimental Néel temperature. In the experiments, the order parameter is determined through the position of the peak in the Fourier-transformed SOC image, with an acquisition time of several seconds. Therefore a measurement of a continuously moving CSS would indeed result in a zero contrast. But the numerical evaluation of the order parameter, which is evaluated through the FFT analysis of the spin configuration of the system on a femtosecond time scale, will continue indicating the existence of the CSS order. An analogous argument, based on rapid thermal fluctuations, was used to explain the absence of magnetic signal using a spin-resolved STM for $B = 0$ T of a sample of Fe chains on the reconstructed $(5 \times 1)$-Ir(001) surface (forming a ferromagnetic cycloidal 120° spin spiral) [41].

To illustrate this effect, we defined a new order parameter $I^{1/2}(\langle M \rangle)$, the square root of maximal intensity of the FFT of the time-averaged magnetization. $I^{1/2}(\langle M \rangle)$ is sensitive to dynamical switching and therefore it is the appropriate parameter to compare with the experiments. Then, we chose a Mn/W(110) nanoisland of $64 \times 64$ spins and simulated the temperature dependence of both order parameters: $I^{1/2}$ and $I^{1/2}(\langle M \rangle)$. The results are summarized in Fig. 5 which clearly shows that $I^{1/2}(\langle M \rangle)$ is sensible to the switching of the cycloidal spin spiral and therefore to the acquisition time ($t_{av}$). If the average time is increased from $t_{av} = 0.1$ ns to $t_{av} = 5.0$ ns the suggested Néel temperature evaluated with the procedure closer to the experiments is reduced by approximately 250 K while $T_N$ estimated by the temperature dependence of $I^{1/2}$ remains practically unchanged.

### D. Scaling/size effects

To investigate the thermal properties of Mn/W(110) further we have also studied the influence of a finite sample size; towards this goal we simulate finite samples using open boundary conditions. We find that the wavelength of the CSS λ periodically oscillates with progressively increased size along

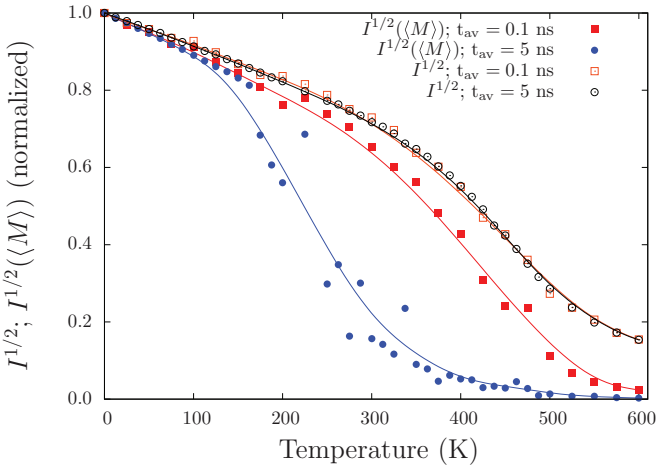


FIG. 5. (Color online) Temperature dependence of the order parameters $I^{1/2}$ (empty symbols) and $I^{1/2}(\langle M\rangle)$ (solid symbols) for two values of the average time $t_{av} = 0.1$–$5.0$ ns. The solid lines are only a guide for the eye.

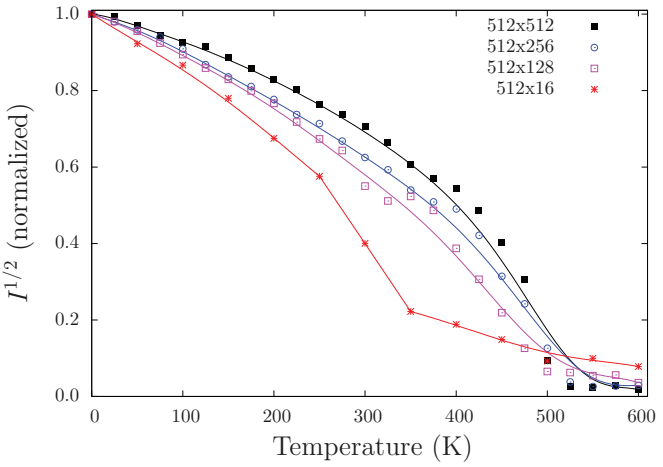


FIG. 6. (Color online) Order parameter as a function of temperature for different sizes in [001] direction (the solid lines are only a guide for the eye).

[1$\bar{1}$0]. The loss of neighbors at the boundaries and its effect on the net-DM interaction leads to pinning effects that explain this variation of the magnitudes of $\lambda$. As can be expected, this effect becomes negligible for sufficiently large systems. For narrow systems (lateral size smaller than half of the wavelength of the CSS in big systems) the wavelength of the CSS considerably increases until it reflects an AFM order. In contrast, a variation of the system size along the [001] direction, i.e. perpendicular to the CSS, had no significant impact on the ground state as obtained in our numerical simulations. We note that while the magnetic order of the system of size $512 \times 16$ still reflects the order of a spin spiral (with identical $\lambda$ as in big systems), the magnetic order of the system of size $16 \times 512$ spins comes closer to an AFM ordering with a slight canting between neighboring moments in each sublattice. The numerical $T_N$ is evaluated through the fitting of the order parameter temperature decay to the analytical expression $(1 - T/T_N)^{\beta}$ being $\beta$ and $T_N$ fitting parameters.

Turning to the thermal behavior, we investigated the effect of the system size on $T_N$ as suggested by the measurements of Sessi *et al.* [15]. For this purpose, lattices with size comparable to the ones used in the experiment were employed. Figure 6 shows the temperature dependence of the CSS order parameter for system sizes varied along [001]. Already for relatively large systems a trend towards slightly reduced $T_N$ can be recognized. This effect becomes even more clear when going to narrower stripes. In contrast, reducing the system size along the [1$\bar{1}$0] direction leaves the thermal dependence of the order parameter largely unaffected (not shown). Both tendencies were observed by Sessi *et al.* [15].

The reduction of $T_N$ in our simulations is partially a finite-size effect: due to the big spatial range for the interactions considered in our model and the very small size of systems, the loss of bonds is significant. As suggested in Ref. [15], the different behavior of $T_N$ when squeezing the system along different directions can also be understood by the different spin stiffnesses: from our *ab initio* calculations we obtained a spin stiffness along [1$\bar{1}$0] 1.5 times larger than that for [001] direction (see also Ref. [1]).

## IV. CONCLUSION

We presented a spin-model suitable to describe the magnetism of a manganese monolayer on the (110) surface of tungsten. The parametrization was based on *ab initio* calculations and included long-ranged relativistic exchange interactions, whereby a fast Fourier transform technique allowed for an economical spin-dynamics simulation.

Our results for the ground-state magnetic configuration of Mn/W(110) agreed remarkably well with measurements, especially the wavelength of the cycloidal spin spiral. We further investigated thermal properties, especially the decay of the magnetic order up to the Néel temperature. Our two main results in this section are as follows: (i) Our experimental as well as numerical results show that up to the Néel temperature no magnetic transition from CSS to an antiferromagnetic state exists and the wavelength of the CSS remains practically constant. (ii) We found that the initial discrepancy between our experimental and numerical estimation of the Néel temperature can be explained by the thermally activated dynamical process in the magnetic state of the CSS.

Additionally for very narrow stripes, the experimentally observed trend that for systems with a reduced size along [001] the Néel temperature decays, while it does not for reduced sizes along the [1$\bar{1}$0] direction, was found in our simulations as well.

## ACKNOWLEDGMENTS

Financial support was provided by the Hungarian National Research Foundation (under Contract No. OTKA 84078) and Deutsche Forschungsgemeinschaft through SFB 767. The work of L.S. was also supported by the European Union and the State of Hungary, cofinanced by the European Social Fund in the framework of TÁMOP 4.2.4. A/2-11-1-2012-0001 "National Excellence Program." M.B. acknowledges funding through Deutsche Forschungsgemeinschaft (BO 1468/22-1).

[1] M. Bode, M. Heide, K. von Bergmann, P. Ferriani, S. Heinze, G. Bihlmayer, A. Kubetzka, O. Pietzsch, S. Blügel, and R. Wiesendanger, Chiral magnetic order at surfaces driven by inversion asymmetry, Nature (London) **447**, 190 (2007).

[2] S. Meckler, N. Mikuszeit, A. Pressler, E. Y. Vedmedenko, O. Pietzsch, and R. Wiesendanger, Real-space observation of a right-rotating inhomogeneous cycloidal spin spiral by spin-polarized scanning tunneling microscopy in a triple axes vector magnet, Phys. Rev. Lett. **103**, 157201 (2009).

[3] A. Balan, P. M. Derlet, A. F. Rodríguez, J. Bansmann, R. Yanes, U. Nowak, A. Kleibert, and F. Nolting, Direct observation of magnetic metastability in individual iron nanoparticles, Phys. Rev. Lett. **112**, 107201 (2014).

[4] M. Bode, Spin-polarized scanning tunnelling microscopy, Rep. Prog. Phys. **66**, 523 (2003).

[5] R. Wiesendanger, Spin mapping at the nanoscale and atomic scale, Rev. Mod. Phys. **81**, 1495 (2009).

[6] R. Wiesendanger, H.-J. Güntherodt, G. Güntherodt, R. J. Gambino, and R. Ruf, Observation of vacuum tunneling of spin-polarized electrons with the scanning tunneling microscope, Phys. Rev. Lett. **65**, 247 (1990).

[7] R. Ravlić, M. Bode, A. Kubetzka, and R. Wiesendanger, Correlation of dislocation and domain structure of Cr(001) investigated by spin-polarized scanning tunneling microscopy, Phys. Rev. B **67**, 174411 (2003).

[8] M. Bode, S. Heinze, A. Kubetzka, O. Pietzsch, M. Hennefarth, M. Getzlaff, R. Wiesendanger, X. Nie, G. Bihlmayer, and S. Blugel, Structural, electronic, and magnetic properties of a Mn monolayer on W(110), Phys. Rev. B **66**, 014425 (2002).

[9] A. Kubetzka, O. Pietzsch, M. Bode, and R. Wiesendanger, Magnetism of nanoscale Fe islands studied by spin-polarized scanning tunneling spectroscopy, Phys. Rev. B **63**, 140407 (2001).

[10] R. Ravlić, M. Bode, and R. Wiesendanger, Correlation of structural and local electronic and magnetic properties of Fe/Cr(001) studied by spin-polarized scanning tunnelling microscopy, J. Phys.: Condens. Matter **15**, S2513 (2003).

[11] F. Meier, K. von Bergmann, P. Ferriani, J. Wiebe, M. Bode, K. Hashimoto, S. Heinze, and R. Wiesendanger, Spin-dependent electronic and magnetic properties of Co nanostructures on Pt(111) studied by spin-resolved scanning tunneling spectroscopy, Phys. Rev. B **74**, 195411 (2006).

[12] A. Kubetzka, O. Pietzsch, M. Bode, and R. Wiesendanger, Spin-polarized scanning tunneling microscopy study of 360° walls in an external magnetic field, Phys. Rev. B **67**, 020401 (2003).

[13] U. Schlickum, N. Janke-Gilman, W. Wulfhekel, and J. Kirschner, Step-induced frustration of antiferromagnetic order in Mn on Fe(001), Phys. Rev. Lett. **92**, 107203 (2004).

[14] A. A. Khajetoorians, J. Wiebe, B. Chilian, and R. Wiesendanger, Realizing all-spin–based logic operations atom by atom, Science **332**, 1062 (2013).

[15] P. Sessi, N. P. Guisinger, J. R. Guest, and M. Bode, Temperature and size dependence of antiferromagnetism in Mn nanostructures, Phys. Rev. Lett. **103**, 167201 (2009).

[16] I. J. Dzyaloshinskii, A thermodynamic theory of "weak" ferromagnetism of antiferromagnetics, J. Phys. Chem. Solids **4**, 241 (1958).

[17] T. Moriya, Anisotropic superexchange interaction and weak ferromagnetism, Phys. Rev. **120**, 91 (1960).

[18] L. Udvardi, A. Antal, L. Szunyogh, A. Buruzs, and P. Weinberger, Magnetic pattern formation on the nanoscale due to relativistic exchange interactions, Physica B **403**, 402 (2008).

[19] V. C. A. Fert and J. Sampaio, Skyrmions on the track, Nat. Nanotechnol. **8**, 152 (2013).

[20] N. Nagaosa and Y. Tokura, Topological properties and dynamics of magnetic skyrmions, Nat. Nanotechnol. **8**, 899 (2013).

[21] R. Yanes, J. Jackson, L. Udvardi, L. Szunyogh, and U. Nowak, Exchange bias driven by Dzyaloshinskii-Moriya interactions, Phys. Rev. Lett. **111**, 217202 (2013).

[22] M. Mochizuki, X. Z. Yu, S. Seki, N. Kanazawa, W. Koshibae, J. Zang, M. Mostovy, Y. Tokura, and N. Nagaosa, Thermally driven ratchet motion of a skyrmion microcrystal and topological magnon Hall effect, Nat. Mater. **13**, 241 (2014).

[23] E. Y. Vedmedenko, L. Udvardi, P. Weinberger, and R. Wiesendanger, Chiral magnetic ordering in two-dimensional ferromagnets with competing Dzyaloshinsky-Moriya interactions, Phys. Rev. B **75**, 104431 (2007).

[24] M. Heide, G. Bihlmayer, and S. Blügel, Dzyaloshinskii-Moriya interaction accounting for the orientation of magnetic domains in ultrathin films: Fe/W(110), Phys. Rev. B **78**, 140403 (2008).

[25] L. Udvardi and L. Szunyogh, Chiral asymmetry of the spin-wave spectra in ultrathin magnetic films, Phys. Rev. Lett. **102**, 207204 (2009).

[26] L. Szunyogh, B. Újfalussy, and P. Weinberger, Magnetic anisotropy of iron multilayers on Au(001): First-principles calculations in terms of the fully relativistic spin-polarized screened KKR method, Phys. Rev. B **51**, 9552 (1995).

[27] B. Gyorffy, A. Pindor, J. Staunton, G. Stocks, and H. Winter, A first-principles theory of ferromagnetic phase transitions in metals, J. Phys. F: Met. Phys. **15**, 1337 (1985).

[28] L. Szunyogh, L. Udvardi, J. Jackson, U. Nowak, and R. Chantrell, Atomistic spin model based on a spin-cluster expansion technique: Application to the $IrMn_3$/Co interface, Phys. Rev. B **83**, 024401 (2011).

[29] A. Deák, L. Szunyogh, and B. Ujfalussy, Thickness-dependent magnetic structure of ultrathin Fe/Ir(001) films: From spin-spiral states toward ferromagnetic order, Phys. Rev. B **84**, 224413 (2011).

[30] E. Simon, K. Palotas, B. Ujfalussy, A. Deák, G. M. Stocks, and L. Szunyogh, Spin-correlations and magnetic structure in an Fe monolayer on 5*d* transition metal surfaces, J. Phys.: Condens. Matter **26**, 186001 (2014).

[31] E. Simon, K. Palotás, L. Rózsa, L. Udvardi, and L. Szunyogh, Formation of magnetic skyrmions with tunable properties in PdFe bilayer deposited on Ir(111), Phys. Rev. B **90**, 094410 (2014).

[32] L. Udvardi, L. Szunyogh, K. Palotás, and P. Weinberger, First-principles relativistic study of spin waves in thin magnetic films, Phys. Rev. B **68**, 104436 (2003).

[33] A. Lyberatos, D. Berkov, and R. Chantrell, A method for the numerical simulation of the thermal magnetization fluctuations in micromagnetics, J. Phys.: Condens. Matter **5**, 8911 (1993).

[34] U. Nowak, in *Micromagnetism*, Handbook of Magnetism and Advanced Magnetic Materials Vol. 2, edited by H. Kronmüller and S. Parkin (Wiley, Chichester, 2007).

[35] J. L. García-Palacios and F. J. Lázaro, Langevin-dynamics study of the dynamical properties of small magnetic particles, Phys. Rev. B **58**, 14937 (1998).

[36] M. Bode, S. Krause, L. Berbil-Bautista, S. Heinze, and R. Wiesendanger, On the preparation and electronic properties of clean W(1 1 0) surfaces, Surf. Sci. **601**, 3308 (2007).

[37] H. J. W. Zandvliet and A. van Houselt, Scanning tunneling spectroscopy, Annu. Rev. Anal. Chem. **2**, 37 (2009).

[38] M. Bode, S. Heinze, A. Kubetzka, O. Pietzsch, X. Nie, G. Bihlmayer, S. Blügel, and R. Wiesendanger, Magnetization-direction-dependent local electronic structure probed by scanning tunneling spectroscopy, Phys. Rev. Lett. **89**, 237205 (2002).

[39] S. Z. Lin, C. Reichhardt, C. D. Batista, and A. Saxena, Particle model for skyrmions in metallic chiral magnets: Dynamics, pinning, and creep, Phys. Rev. B **87**, 214419 (2013).

[40] R. E. Troncoso and A. S. Núñez, Thermally assisted current-driven skyrmion motion, Phys. Rev. B **89**, 224403 (2014).

[41] M. Menzel, A. Kubetzka, K. von Bergmann, and R. Wiesendanger, Parity effects in 120° spin spirals, Phys. Rev. Lett. **112**, 047204 (2014).